A novel versatile animal-free 3D tool for rapid low-cost assessment of immunodiagnostic microneedles*

Stella Totti[a], Keng Wooi Ng[b,c], Lorraine Dale[c], Guoping Lian[a,d], Tao Chen[a], Eirini G. Velliou[a,†]

[a]Bioprocess and Biochemical Engineering Group (BioProChem), Department of Chemical and Process Engineering, University of Surrey, Guildford, GU2 7XH, UK
[b]School of Pharmacy, Faculty of Medical Sciences, Newcastle University, Newcastle upon Tyne, NE1 7RU, UK
[c]School of Pharmacy and Biomolecular Sciences, University of Brighton, Brighton, BN2 4GJ, UK
[d]Unilever R&D Colworth, Colworth Park, Sherbrook, Bedforshire, MK44 1LQ, UK

Microneedle devices offer minimally invasive and rapid biomarker extraction from the skin. However, the lack of effective assessment tools for such microneedle devices can delay their development into useful clinical applications. Traditionally, the microneedle performance is evaluated i) in vivo, using animal models, ii) ex vivo, on excised human or animal skin or iii) in vitro, using homogenised solutions with the target antigen to model the interstitial fluid. In vivo and ex vivo models are considered the gold-standard approach for the evaluation of microneedle devices because of their structural composition, however they do exhibit limitations. More specifically, they have limited availability and they present batch-to-batch variations depending on the skin origin. Furthermore, their use rises ethical concerns regarding compliance with the globally accepted 3Rs principle of reducing the use of animals for research purposes. At the same time, in vitro models fail to accurately mimic the structure and the mechanical integrity of the skin tissue that surrounds the interstitial fluid. In this study, we introduce for the first time an animal-free, mechanically robust, 3D scaffold that has great potential as an accurate in vitro evaluation tool for immunodiagnostic microneedle devices. More specifically, we

*To appear in final edited form as: Totti S, Ng KW, Dale L, Lian G, Chen T, Velliou EG, A novel versatile animal-free 3D tool for rapid low-cost assessment of immunodiagnostic microneedles, Sensors and Actuators: B. Chemical (2019), https://doi.org/10.1016/j.snb.2019.126652
†Corresponding author: e.velliou@surrey.ac.uk

demonstrate, for the first time, successful extraction and detection of a melanoma biomarker (S100B) using immunodiagnostic microneedles in the 3D culture system. Melanoma cells (A375) were cultured and expanded for 35 days in the highly porous polymeric scaffold followed by in situ capture of S100B with the microneedle device. Scanning electron microscopy showed a close resemblance between the 3D scaffold and human skin in terms of internal structure and porosity. The microneedle device detected S100B in the scaffold (with a detection pattern similar to the positive controls), while the biomarker was not detected in the surrounding liquid supernatants. Our findings demonstrate the great potential of this animal-free 3D tool for rapid and low-cost evaluation of microneedle devices.

Keywords: Microneedles, diagnostic device, biomarker detection, S100B, melanoma, three-dimensional in vitro model

Highlights

- A 3D animal-free tool for assessment of immunodiagnostic microneedles is introduced.
- A 3D highly porous structure which mimics the porosity of skin is manufactured.
- S100B detection with microneedles in a novel 3D melanoma culture is evaluated.

1 Introduction

In recent years, a range of solid and hollow microneedles (MNs) have been developed for dermal drug delivery and diagnostic applications [1–13]. As a dermal diagnostic device, MNs are advantageous over conventional methods for skin biomarker extraction. Traditional biomarker extraction techniques necessitate the collection of a significant volume (several millilitres) of biofluids, and are therefore limited to liquid tissues (e.g. blood and urine). In this regard, detection of biomarkers on skin, which is a solid tissue, remains challenging due to lack of efficient sampling and detection methods [14–17]. Instead, invasive skin biopsies have been used routinely, but they cause significant physical trauma and mental distress to the patient, as well as requiring extensive histological processing and patient aftercare [16,18–20]. Therefore, MNs offer an attractive alternative to skin biopsies, as they can penetrate the dermal tissue in a minimally invasive manner, causing minimal tissue damage and little to no pain [21, 22]. Additionally, MNs can easily access the interstitial fluid (ISF) that surrounds the tissue cells, making biomarker capturing in the ISF possible [14]. This is of great importance, especially for the early detection of malignant diseases, as the cancer biomarker concentration in the tumour ISF is anticipated to be significantly higher than in the plasma [23].

Current assessment of MNs detection performance is mainly carried out (i) in vivo using animal models, (ii) ex vivo using excised human or animal skin, or (iii) in vitro using liquid biomarker solutions [8–12, 24].

In vivo models are not ideal due to ethical, economic and practical reasons. Moreover, animal-free models are strongly encouraged by the European legislation under the 3R's principle of reducing, refining and replacing animal experimentation whenever possible [25, 26]. Furthermore, excised skin ex vivo models entail their own ethical considerations, as well as being expensive and limited in availability [27, 28]. Excised human skin tumour samples are especially difficult to obtain for pre-clinical experimentation, as they are used for disease diagnosis. Among a wide range of animal models that have been suggested as a replacement for human skin, porcine skin is the most relevant, as it shows striking histological and biochemical similarities to the human skin [29, 30]. Nonetheless, porcine skin has been reported to exhibit higher permeability than human skin [31–33]. Finally, the inherent interspecies variations and batch-to-batch variability depending on the skin origin may complicate the interpretation of experimental results [27, 34].

Current in vitro models for microneedle (MN) assessment consist of liquid biomarker solutions that are used as a surrogate of the skin ISF. These homogenous solutions contain specific concentrations of the target biomarker to be extracted by the MNs. However, the homogenous solutions are unable to recapitulate the 3D structure and porosity of the actual skin tissue, therefore failing to act as accurate skin surrogates. Hence, the liquid solutions might give a preliminary indication of the detection performance of the MN devices, but more physiologically relevant evaluation models are needed. More specifically, to develop realistic models for the assessment of the MNs, it is essential to mimic the skin tissue properties (i.e. porosity, structure, elasticity, oxygenation level). Those properties are different for each individual and are influenced by numerous factors, including, gender, anatomical site, tissue depth, level of hydration and age [35–40]. For example, the aging skin is characterised by increased stiffness due to the deposition and fragmentation of collagen [41]. Also, the pore size of the human skin increases with distance from the skin surface [42]. Although the oxygenation levels in the skin tissue are difficult to measure accurately, the skin is considered a mildly hypoxic tissue [40, 43, 44]. Therefore, it is important to develop easily tuneable and versatile in vitro skin tools for MN evaluation, which can easily capture the skin properties.

Three-dimensional (3D) biomaterial-based structures can provide a more realistic structure/architecture for cells to grow in vitro, enhancing cell-cell spatial interactions and providing a tissue-specific internal structure. Therefore, such 3D constructs could be promising tools for the evaluation of MN devices [45–49]. However, to the authors' knowledge, only one study has explored the potential of a 3D tool for this purpose. Omolu et al. developed a 3D in vitro tool to test MN rollers for drug delivery purposes [4]. The in vitro tool consisted of a synthetic membrane placed on the top of collagen gels seeded with primary fibroblasts. However, the skin structural and mechanical integrity is still lacking in currently available 3D systems. The use of polymeric foam type scaffolds of controlled porosity could be a promising approach to recapitulate the human skin internal structure and stiffness. These scaffolds have tuneable properties (i.e. porosity, stiffness) to mimic the structural variability of human skin [50]. Additionally, the internal pore network of these scaffolds provide physical surfaces for the cells to bind and interact with each other. Importantly, the porous network facilitates nutrient and oxygen diffusion, thus enabling the long-term culture of the cells in vitro [48–50].

In this work, we present for the first time, a novel, animal-free, mechanically robust, versatile 3D polyurethane (PU) scaffold that can be used as a tuneable low-cost tool for assessing immunodiagnostic MNs able to capture specific biomarkers in the skin. Metastatic melanoma cells were cultured in the scaffold and S100B, a well-established intra-tumoural biomarker for cutaneous melanoma [51, 52], was captured in situ with MNs. Malignant melanoma is the most lethal skin cancer, with a 5-year survival rate of just 20% [53, 54]. The most effective treatment for melanoma is surgical resection, and early detection greatly enhances prognosis. An elevated serum 100B concentration is not only associated with malignant melanoma but provides prognostic value as well [55], which underpins its use as the target biomarker in this study

2 Materials and methods

2.1 Fabrication and characterisation of immunodiagnostic MN devices

Polylactic acid (PLA)-based immunodiagnostic MN devices were fabricated and characterised as described previously [12]. Briefly, PLA (Maker Bot, USA) was melted into a polydimethylsiloxane micromould at 200°C and 100 mbar. The PLA was allowed to solidify in the micromould following cooling to room temperature. The resultant PLA MN device was ejected from the micromould and immersed in 6% w/v hexamethylenediamine (prepared in propan-1-ol) at 50°C for 90 s, followed by immersion in 2% w/w aqueous glutaraldehyde at room temperature for 3 h to facilitate covalent antibody immobilisation. The MN devices thus prepared were then washed with deionised water, air-dried, and coated in a multiplex format with (i) an anti-human S100B monoclonal antibody (clone 8B10, used at 1 mg/mL; Bio-Rad, UK), (ii) 5% w/v bovine serum albumin (BSA; prepared in phosphate buffered saline pH 7.4 with 0.05% w/v Tween® 20) as negative control, and (iii) horseradish peroxidase (HRP) as positive control. Coating was achieved by dipping each MN individually into the coating solution 20 times, with 1–2 min drying time in between. Coated MN arrays were immersed in 5% w/v BSA solution, at 4°C for 24 h, to block non-specific binding sites. The coated MNs were then air-dried, ready for use in biomarker detection experiments. The MN devices were observed under a CETI Steddy stereomicroscope (Medline Scientific, UK). Images were recorded using a 3 Mpx digital camera (Medline Scientific, UK). Measurements of the MNs were performed on the images using the ImageJ software version 1.52k (National Institutes of Health, USA), calibrated against the image of a stage micrometer (Cole-Palmer, USA) at the same magnification.

2.2 Fabrication and sterilisation of the scaffolds

The PU scaffolds were fabricated by thermally induced phase separation (TIPS), as previously described [49, 56, 57]. Briefly, PU beads (Noveon, Belgium) were dissolved in dioxane (5% w/v) (99.8% anhydrous pure, Sigma-Aldrich, UK) and the solution was quenched at −80°C for 3 h. Thereafter, the solvent was removed by freeze-drying in an ethylene glycol (EG) bath at −15°C under 0.01 bar vacuum pressure. The scaffolds

were cut into $5 \times 5 \times 2.5\,\text{mm}^3$ cuboids. The thickness of the scaffolds (2.5 mm) is a good representation of the human epidermis and dermis thickness [58–61]. The elastic modulus of the scaffolds, as evaluated with compression tests, was 33.17 ± 2.08 kPa. The elastic modulus of the polymeric scaffolds lies within the elastic properties of the human skin, which vary significantly depending on the gender, the age and the anatomical site [60, 62]. The average pore size that was measured previously was 100–150 μm and the porosity 85–90% [56]. Sterilisation of the scaffolds took place by washing them with 70% v/v ethanol solution for 3 h, followed by exposure to a UV/ozone generator for 10 min (BioForce Nanosciences, USA).

2.3 3D melanoma cell culture

The human malignant melanoma cell line A375 (Sigma-Aldrich UK, ECAAC 88113005) was expanded in tissue culture plastic flasks (Fisher Scientific, UK) in Dulbecco's modified Eagle's medium (DMEM) with 4.5 g/L glucose (Lonza, UK), supplemented with 15% v/v heat inactivated foetal bovine serum (FBS; Fisher Scientific, UK), 100 U/mL penicillin/streptomycin (Sigma-Aldrich, UK) and 2 mM L-glutamine (Sigma-Aldrich, UK). Mycoplasma negative cultures were ensured by regular mycoplasma screening tests (Lonza, UK). 10^6 cells were seeded in each scaffold. Thereafter, the scaffolds were placed in 24-well plates and allowed to settle for 30 min in an incubator at 37°C in 5% CO_2 and 95% air. Afterwards, 1.5 mL of the cell culture medium was added in each well and the scaffolds were kept in an incubator at 37°C, 5% CO_2 and 95% air. Cell viability was evaluated with live/dead staining (section 2.5) on day 5 and 35 of culture. The cell culture medium was replenished every two to three days. To avoid cell confluency at the bottom of the wells resulting from cells exiting the scaffolds, samples were placed in a new well-plate on a weekly basis. Every week, the spent medium from at least two independent scaffolds was aspirated, centrifuged at $300 \times g$ for 10 min to remove any remaining debris and stored at −20°C for further analysis.

2.4 Scanning electron microscopy

The 3D scaffolds were sectioned and the cell distribution and adhesion on/in the pores of the matrix was observed with scanning electron microscopy (SEM). The specimens were collected at the culture endpoint (day 35), snap-frozen in liquid nitrogen for 15 min and then preserved in −80°C until fixation. At fixation, samples where sectioned approximately in the middle with a razor and then directly immersed in 4% v/v cold formaldehyde solution (Sigma-Aldrich, UK) for 2 h at room temperature. Thereafter, post fixation took place including 2 washing steps with PBS for 15 min each, followed by 4 washing steps with deionized water for 15 min each to ensure removal of the residual crystals. Afterwards, the scaffold sections were air-dried overnight in an aseptic environment. The specimens were sputter coated with gold in an argon atmosphere 24 h prior to the SEM imaging. The SEM was performed on a JEOL 7100F (JEOL USA, MA, USA) microscope at different magnifications.

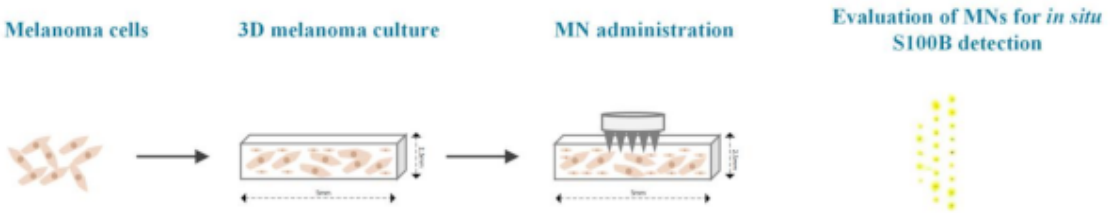

Figure 1: Schematic representation of S100B detection in the 3D melanoma culture with the immunodiagnostic MN device.

2.5 In situ live/dead staining viability assay

Cell viability in the scaffolds was visualised with confocal laser scanning microscopy (CLSM). As per section 2.4, scaffolds were collected at the beginning of the culture (day 5) and at the culture end point (day 35), snap-frozen in liquid nitrogen for 15 min and preserved at −80°C. After sectioning, the samples were incubated with calcein AM (2 μM; Life Technologies, Paisley, UK) and ethidium homodimer-1 (4 μM; Life Technologies) in culture medium for 1 h at 37°C. The presence of live (green) and dead (red) cells was evaluated with a Nikon Ti-Eclipse inverted confocal microscope (Nikon Instruments, Europe) and processed with Nikon software (Nikon Instruments, Europe).

2.6 Biomarker capture and detection

The immunodiagnostic MN devices were administered on the 3D scaffolds seeded with melanoma cells on day 35 of culture, ensuring penetration of the specimens, and incubated in situ for 3 h (Figure 1). Meanwhile, separate MN devices were incubated for 2 h with: (i) supernatants of the 3D-scaffolded melanocyte culture at the same time point (day 35); (ii) 100 μg/mL recombinant human S100B (Abcam, UK) in freshly prepared culture medium as the positive control; (iii) freshly prepared culture medium without S100B as negative control. Captured S100B was detected using the blotting method, as previously described [12]. Briefly, MN devices were washed thoroughly with the wash buffer (PBS with 0.05% w/v Tween® 20) and incubated with 2 μg/mL HRP-conjugated anti-human S100B detection antibody (clone 6G1; Abcam, UK) for 1 h. Thereafter, the MN devices were washed thoroughly with the wash buffer again and air-dried. The MN devices were then placed on chromatography paper wetted with 1.6 mg/mL o-phenylenediamine (OPD) solution (prepared in 50 mM phosphate citrate buffer containing 0.03% w/v $NaBO_3$, pH 5.0), ensuring contact between the MN tips and the paper by applying gentle pressure constantly for 30 min. The enzymatic conversion of OPD by HRP (where present) at points of contact between the MN tips and the OPD-wetted paper would produce a yellow colouration and a blot pattern corresponding to the positions of the MNs. By comparing the blot pattern with the coating map, S100B capture was determined.

2.7 Serum negativity validation

A validation study was performed to verify that any S100B apparently detected by the MNs had originated from the melanoma cells and not due to cross-reactivity with unspecified FBS constituents (e.g. bovine S100B) present in the cell culture medium. Sequence homology between human S100B (GenBank accession no. AAH01766.1) and bovine S100B (GenBank accession no. ABA39829.1) was analysed using the BLASTp sequence analysis tool (version 2.8.1; https://blast.ncbi.nlm.nih.gov) [63]. In addition, a conventional sandwich enzyme-linked immunosorbent assay (ELISA) was performed using the same assay reagents as those used with the MN device. A 96-well microtitre plate was first coated with 100 μL of the anti-S100B capture antibody (2 μg/mL, prepared in carbonate buffer, pH 9.6) per well, at 4°C overnight. The capture antibody solution was removed and the wells incubated with the blocking buffer, again at 4°C overnight, to block non-specific binding sites. The wells were emptied and incubated for 2 h, at room temperature, with 100 μL of serially diluted recombinant S100B solutions in high-glucose DMEM, with or without 15% v/v FBS. Following thorough washout of the wells with the wash buffer, 100 μL of the HRP-conjugated detection antibody (2 μg/mL) was added to each well and incubated for 1 h. The wells were then thoroughly washed out again with the wash buffer and incubated with 100 μL of the OPD solution for 20–30 min. The absorbance of the OPD solution was measured at 450 nm on a UVM 340 microplate reader (Asys Hitech, Austria). Data from 5 independent experiments were analysed. Since each assay varied slightly in terms of reagent incubation time and the rate at which the colour signal developed from OPD, in collating the results, the normalised signal was calculated according to Equation 1.

$$\text{Normalised signal } (\%) = \frac{A - A_{\text{min}}}{A_{\text{max}} - A_{\text{min}}} \times 100 \tag{1}$$

Where, A is the absorbance of any given sample, whilst A_{min} and A_{max} denote the minimum and maximum absorbance amongst all samples tested in the same experiment, respectively.

3 Results and discussion

Melanoma is the most lethal skin cancer and the most efficient treatment for it is early diagnosis followed by surgical resection before metastasis [64]. A MN device that can detect melanoma biomarkers in the skin easily and rapidly can enable melanoma screening and early diagnosis at the point of care. In this study, we report for the first time a reproducible, animal-free, inexpensive scaffolding tool to rapidly assess the detection of a melanoma biomarker in vitro using a minimally-invasive MN device. To the authors' knowledge, this is also the first report of a MN device successfully capturing a cancer biomarker (S100B) from a 3D culture of melanoma cells.

3.1 Evaluation of 3D melanoma culture performance prior to MN administration

We have developed a highly porous polyurethane based scaffold which was used as a basis to grow/expand malignant skin cell lines in 3D [49, 57]. This polymeric scaffold was chosen because its internal structure and porous configuration (Figure 2 (a)) closely resemble the human skin (Figure 2 (b)). Additionally, the capability to fine-tune the scaffold's mechanical properties (stiffness, elasticity and porosity, by varying known TIPS parameters) is advantageous for in vitro skin studies, as it enables similar variations in human skin properties to be simulated [35–39, 42].

To evaluate the growth of melanoma cells in the 3D scaffold, 10^6 melanoma cells were seeded in the PU matrix and cultured for 35 days. The cell distribution within the scaffold was evaluated with SEM. The micrographs (Figure 2 (c-d)) indicate that the A375 cells retained their typical epithelial morphology within the scaffold [65–67]. Additionally, the viability of the 3D melanoma culture remained high for 35 days, as evaluated by a live/dead viability assay (Figure 2 (e–f)). The cells were distributed as single cells at the beginning of the culture (Figure 2 (e)), however as the culture evolved the cells proliferated up to day 35 in the 3D model and formed larger cellular aggregates (Figure 2 (f)). It is worth noting that 3D in vitro melanoma cultures typically last for 2 weeks [67–70]. Apart from Hill et al. whose melanoma culture lasted for 35 days, using a 200 μm-thick, commercially available polystyrene 3D scaffold, our scaffold also demonstrated excellent cellular viability and growth characteristics maintenance for 35 days [71, 72]. This enhanced scaffold thickness, as well as the ability to tune it, is important because tumour thickness increases with disease progression, and even the earliest stage (T1) cutaneous melanoma can be up to 1 mm thick from the epidermal surface [73]. The thickness of our 3D culture system (2.5 mm) corresponds to the invasion depth of a T3 tumour. It not only provides the ability to mimic the full thickness of cutaneous melanoma beyond T1, but will also accommodate full insertion of MNs longer than 200 μm.

3.2 S100B capture in the 3D scaffold with MNs

3.2.1 MN device characteristics

Once the high viability of the melanoma cells in the 3D model was confirmed, the potential to use this system as an in vitro tool for S100B detection with the MN device was evaluated. The MN devices used in the positive control experiments had 35 MNs per device, while the rest had 34 MNs per device. These were arranged in 5 rows consisting of 5, 8, 9/8, 8 and 5 MNs, respectively (Figure 3 (a)). In all cases, the MNs were conical with a slightly convex surface, approximately 1 mm long and 230 μm in base diameter. The coating map of the MNs is presented in Figure 3 (a).

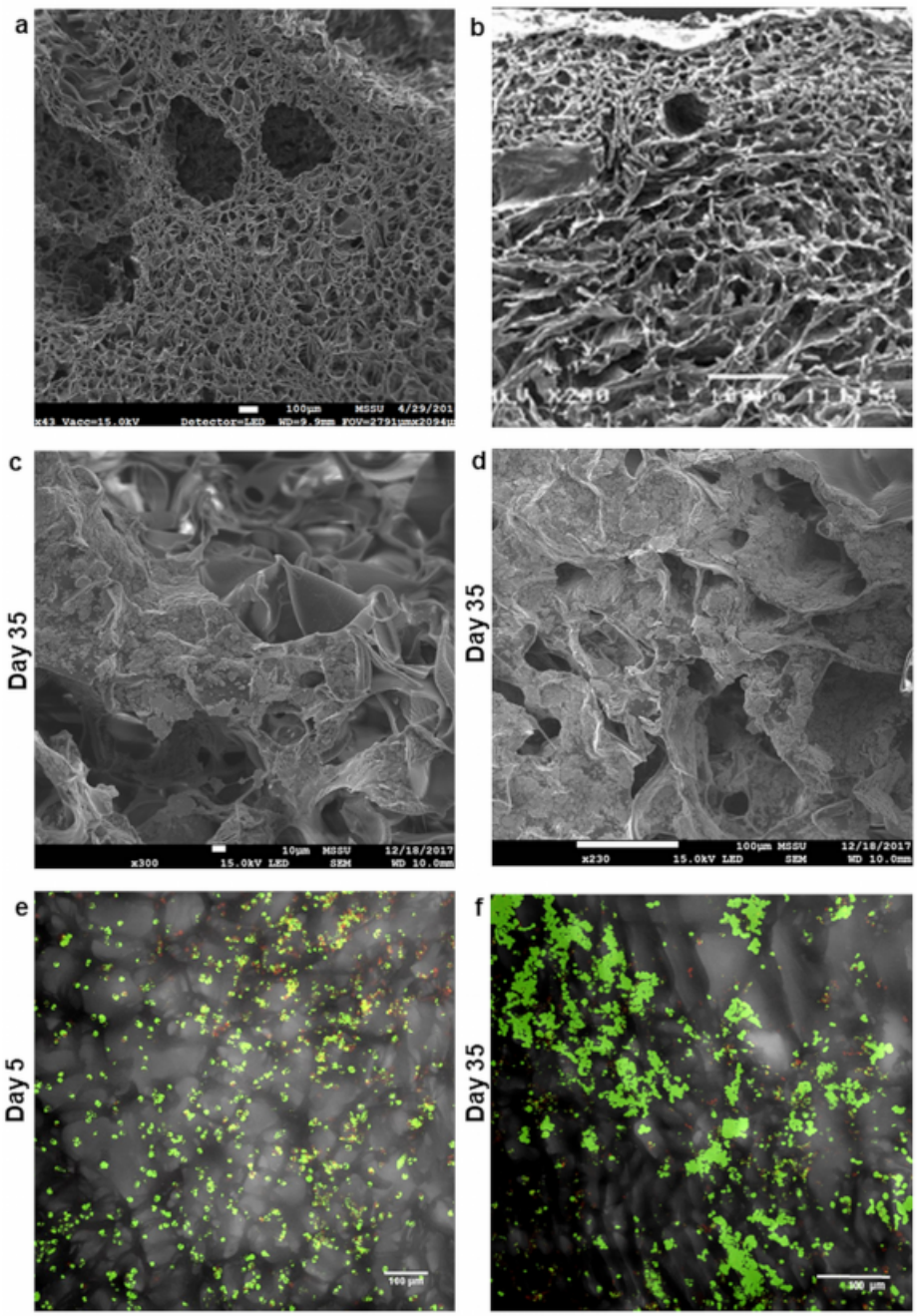

Figure 2: Evaluation of the 3D melanoma culture. SEM images of (a) the microporous 3D scaffold without cells; (b) human skin (adapted from Loh and Choong, 2013 [42]; Image used with the permission of the publisher). (c–d) A375 melanocytes in sections of the scaffold at day 35 of culture. (e–f) Visualization of A375 viability in the scaffold with fluorescence live (green, calcein AM) and dead (red, ethidium homodimer-1) viability assay at (e) day 5 of culture and (f) day 35 of culture.

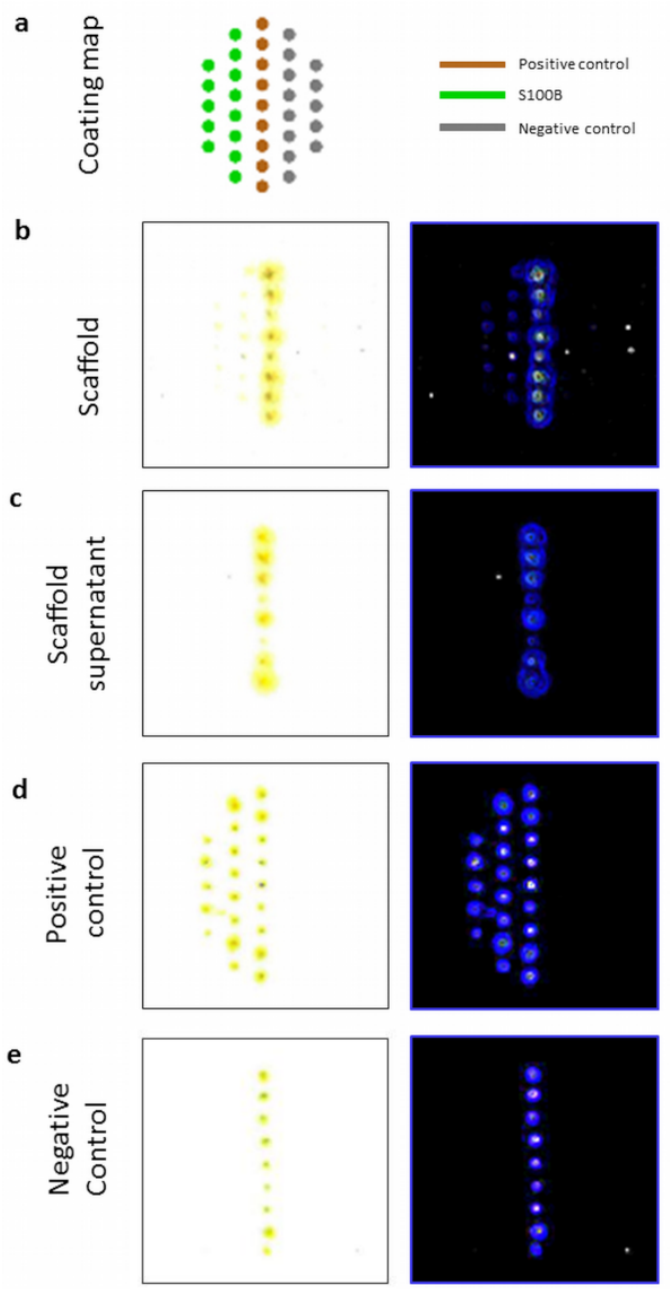

Figure 3: (a) Coating map of the MN device. S100B detection with the blotting technique in (b) the 3D scaffold, (c) the 3D melanoma culture supernatants, (d) the positive control comprising 100 μg/mL S100B in fresh culture medium, (e) the negative control comprising fresh culture medium only. (b–e) Images on the left show the blots adjusted for brightness and contrast only; images on the right show the corresponding blots with the blot patterns accentuated using the "Edge Detect" filter in the GNU Image Manipulation Program (GIMP, version 2.8.18; https://www.gimp.org).

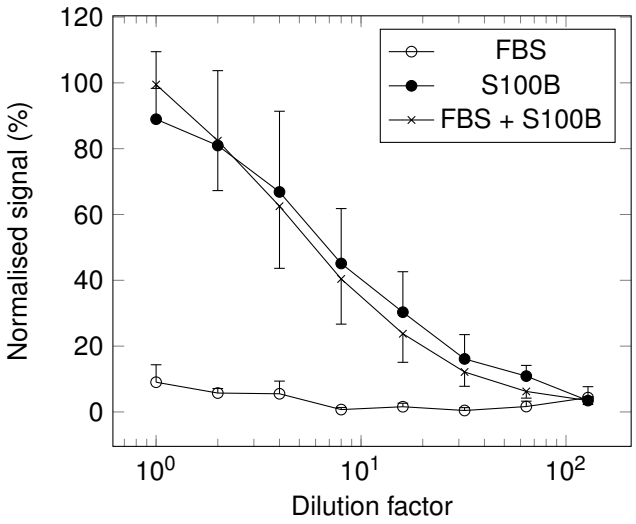

Figure 4: ELISA calibration plots showing normalised signal (Equation 1) against dilution factor for DMEM supplemented with FBS and/or S100B. The plots show that FBS constituents in the cell culture medium did not cross-react with the antibodies used with MN devices, thus confirming the melanoma cells as the source of the S100B detected. Data are mean ± standard deviations from 5 independent experiments. Error bars are staggered for clarity.

3.2.2 In situ S100B capture on the 3D melanoma culture and culture supernatants

Figure 3 (b) shows the blotting patterns of S100B detection in the scaffold, which corresponds to the positions of the MNs. The MN device captured S100B from the 3D melanoma cell culture, producing a clear, visible colour signal similar to the positive control (Figure 3 (d)). The results show that the MN devices were sensitive and the S100B detection was specific. To our knowledge, this is the first time that S100B has been detected by MNs in a 3D biomaterial-based melanoma culture. Considering that our sequence homology analysis had shown human S100B to be 97% identical and 100% similar to bovine S100B, we were prompted to investigate potential cross-reactivity between the antibodies used and FBS, by examining the dose-response relationship between FBS supplementation and the signal produced in a conventional (plate-based) ELISA. Our results demonstrate that FBS did not produce a false positive in the assay, so cross-reactivity can be ruled out (Figure 4). We therefore conclude that the S100B detected by the MN devices originated from the melanoma cells in the 3D scaffold. S100B is over-expressed in malignant melanoma and belongs to the S100 protein family. Dysregulation of the S100 proteins is a characteristic of many cancers [74]. Intra-tumoural S100B is an established histological marker in the diagnosis of cutaneous melanoma, whilst elevated serum S100B concentrations are associated with metastatic melanoma, with some studies reporting prognostic value [75]. However, the S100 proteins are highly conserved among vertebrates [76–78]. At present, the exact intra-tumoural (interstitial) S100B

concentration in melanoma is unclear, but inferences may be made from documented serum concentrations. In melanoma patients, serum S100B concentrations of several hundred pg/mL have been reported, while for healthy individuals the concentration range is 20–80 pg/mL [79–81]. Assuming that the elevated serum S100B concentration originates from the primary tumour, and that the release of S100B from the tumour into the serum tends towards a concentration equilibrium, then the intra-tumoural S100B concentration can be estimated to be in the order of at least several hundred pg/mL. A similar MN device from our laboratory has previously detected a different target antigen at 10 pg/mL, so a suitable detection limit for intra-tumoural S100B seems achievable with the MN approach. S100B capture with the MNs was also attempted on the 3D culture supernatants in order to compare the testing capacity of the 3D model over the culture spent medium [12]. However, as it is indicated in Figure 3 (c), S100B gradients were not detected in the 3D scaffold supernatants. This might be attributed to S100B concentration gradient existence inside of the scaffold and outside. Typically, higher biomarker concentrations are observed closer to the cells that produce them [23, 82]. Additionally, the presence of the scaffold matrix is likely to have slowed down the diffusion of the S100B in the culture medium, allowing an even higher concentration gradient to build up. Nonetheless, the 3D melanoma scaffold is likely to mimic the diffusion gradients of biomarkers through the skin occurring in vivo, an important feature for MN assessment [83].

Overall, the findings highlight that our scaffolding tool can be an animal-free, in vitro tool to test MN devices for diagnostic applications, offering many advantages over other systems currently in use. More specifically, the scaffold tool: (i) is reproducible without batch-to-batch variations, (ii) is easily tuneable in terms of their mechanical properties, internal architecture and porosity to simulate the 3D structure, mechanical properties and porosity of the human skin (Figure 2 (a–b)), and (iii) can be fabricated at low cost [35, 42, 49, 56, 57, 60, 84].

4 Conclusions

In this study, a 3D biomaterial-based scaffold was used as an in vitro tool for evaluating an immunodiagnostic MN device for S100B detection. We have demonstrated, for the first time, the use of the 3D polyurethane scaffold as an animal-free melanoma surrogate for screening and evaluating immunodiagnostic microneedles. The 3D scaffold has a similar internal structure and porosity to human skin. Furthermore, the high tuneability of the scaffold properties (i.e. porosity, elasticity, biochemical composition, oxygenation levels etc.) is beneficial in order to recapitulate the in vivo variability in these properties. Melanoma cells were able to grow in the 3D scaffold for 35 days, the longest yet reported for in vitro melanoma cell culture. Furthermore, the melanoma marker S100B was successfully detected using a novel immunodiagnostic MN device on the in vitro tool. Admittedly, the performance of the MN device may vary depending on various factors, such as the target protein, the extracellular matrix environment, the assay reagents and the detection method. Whilst further studies will need to fully assess the performance of

the MN device for S100B detection, this work has demonstrated the great potential of the 3D-scaffolding tool in facilitating that process. Overall, our 3D scaffolding tool can be used as an inexpensive, animal-free, reproducible model for validation/screening of novel diagnostic devices.

Acknowledgements

This work was supported by the Chemical and Process Engineering Department of the University of Surrey as well as an Impact Acceleration Grant (IAA-KN9149C) of the University of Surrey, an IAA–EPSRC Grant (RN0281J) and the Royal Society. It was also supported by the School of Pharmacy (Newcastle University), School of Pharmacy and Biomolecular Sciences (University of Brighton), as well as a University of Brighton Rising Stars Award to KWN.

Biographies

Stella Totti is a postdoctoral researcher at the Department of Chemical and Process Engineering of the University of Surrey (UK). She received her PhD from the University of Surrey (UK) and her MEng from the Aristotle University of Thessaloniki (AUTH) in Greece. Her research focuses on cancer tissue engineering, transdermal delivery of active compounds, biomaterial and nanomaterial development and characterisation, high-throughput (drug and radiotherapy) screening, in situ biomarker monitoring with advanced imaging techniques.

Keng Wooi Ng is a lecturer at Newcastle University. He received his MPharm and PhD from Cardiff University (UK), and trained as a postdoctoral researcher at Imperial College London (UK) and University of Reading (UK). He accepted a lectureship at University of Brighton (UK) in 2014 and moved to Newcastle University in 2017. His research focuses on developing novel diagnostic and drug delivery technologies for the skin. Recent works include microneedle biosensors, nanomedicines and skin penetration enhancement using chemical penetration enhancers.

Lorraine Dale has a BSc in Cell and Molecular Biology from Kings College London. She completed her MSc in Biomedical Sciences from University of Brighton in 2017, where she researched a diagnostic microneedle device for melanoma biomarker detection in the skin, under the supervision of Dr Keng Wooi Ng. She is currently 24quality control and compliance co-ordinator at the Agora fertility clinic in Brighton, and a visiting researcher at University of Brighton where she continues to work on immunodetection of melanoma biomarkers.

Guoping Lian has a joint appointment as Science Leader at Unilever R&D Colworth (80%) and Professor at the Department of Chemical and Process Engineering of University of Surrey. His main research interest is in multi-scale computational methods applied to (a) pharmacokinetics of transdermal bioavailability and (b)

complex microstructures, properties and processes of multiphase granules, emulsions and dispersions.

Tao Chen is a senior lecturer at the University of Surrey. He received his BEng and MEng from Tsinghua University, China, and PhD from Newcastle University, UK, and trained as a postdoctoral researcher at Newcastle University. Prior to joining the University of Surrey in 2011, he had been an assistant professor at Nanyang Technological University, Singapore. His research focuses on process systems engineering, developing computational models to help understand and optimise drug delivery and other chemical and biological processes.

Eirini Velliou is Senior Lecturer (Associate Professor) of Bioprocess & Tissue Engineering, Principal Investigator and Founder of the Bioprocess and Biochemical Engineering group (BioProChem) in the Department of Chemical and Process 25Engineering at the University of Surrey in the United Kingdom. Eirini holds a PhD from KULeuven, Belgium and an MEng in Chemical Engineering from the National Technical University of Athens, Greece. Her research focus falls within the engineering and validation of novel biomaterial based in vitro platforms for studying various biological systems and diseases, i.e., cancer, stem cells, formulation/communication of bacterial communities and bacterial-host interactions. Furthermore, she is particularly interested on the response and adaptation/resistance of biological systems to environmental stress. Eirini joined the University of Surrey in September 2014 after postdoctoral appointments at Imperial College London and at the Bioengineering Group of the Earth and Life Institute (ELI) of the Université Université Catholique de Louvain (UCL) in Louvain-la-Neuve, Belgium.

References

[1] A. Nayak, D.B. Das, Potential of biodegradable microneedles as a transdermal delivery vehicle for lidocaine, Biotechnol Lett, 35 (2013) 1351–63.

[2] J. Chen, W. Huang, Z. Huang, S. Liu, Y. Ye, Q. Li, et al., Fabrication of Tip-Dissolving Microneedles for Transdermal Drug Delivery of Meloxicam, AAPS PharmSciTech, 19 (2018) 1141–51.

[3] E. Larrañeta, S. Stewart, S.J. Fallows, L.L. Birkhäuer, M.T.C. McCrudden, A.D. Woolfson, et al., A facile system to evaluate in vitro drug release from dissolving microneedle arrays, Int J Pharm, 497 (2016) 62–9.

[4] A. Omolu, M. Bailly, R.M. Day, Assessment of solid microneedle rollers to enhance transmembrane delivery of doxycycline and inhibition of MMP activity, Drug Deliv, 24 (2017) 942–51.

[5] S. Liu, M.-n. Jin, Y.-s. Quan, F. Kamiyama, H. Katsumi, T. Sakane, et al., The development and characteristics of novel microneedle arrays fabricated from hyaluronic

acid, and their application in the transdermal delivery of insulin, J Control Release, 161 (2012) 933–41.

[6] L.M. Strambini, A. Longo, A. Diligenti, G. Barillaro, A minimally invasive microchip for transdermal injection/sampling applications, Lab Chip, 12 (2012) 3370–9.

[7] A. Bhargav, D.A. Muller, M.A.F. Kendall, S.R. Corrie, Surface Modifications of Microprojection Arrays for Improved Biomarker Capture in the Skin of Live Mice, ACS App Materi Interfaces, 4 (2012) 2483–9.

[8] E. Caffarel-Salvador, A.J. Brady, E. Eltayib, T. Meng, A. Alonso-Vicente, P. Gonzalez-Vazquez, et al., Hydrogel-Forming Microneedle Arrays Allow Detection of Drugs and Glucose In Vivo: Potential for Use in Diagnosis and Therapeutic Drug Monitoring, PLoS One, 10 (2015) e0145644.

[9] J.W. Coffey, S.R. Corrie, M.A. Kendall, Early circulating biomarker detection using a wearable microprojection array skin patch, Biomaterials, 34 (2013) 9572–83.

[10] K.T. Lee, D.A. Muller, J.W. Coffey, K.J. Robinson, J.S. McCarthy, M.A.F. Kendall, et al., Capture of the Circulating Plasmodium falciparum Biomarker HRP2 in a Multiplexed Format via a Wearable Skin Patch, Analyt Chem, 86 (2014) 10474–83.

[11] D.A. Muller, S.R. Corrie, J. Coffey, P.R. Young, M.A. Kendall, Surface Modified Microprojection Arrays for the Selective Extraction of the Dengue Virus NS1 Protein As a Marker for Disease, Analyt Chem, 84 (2012) 3262–8.

[12] K.W. Ng, W.M. Lau, A.C. Williams, Towards pain-free diagnosis of skin diseases through multiplexed microneedles: biomarker extraction and detection using a highly sensitive blotting method, Drug Deliv Transl Res, 5 (2015) 387–96.

[13] P. Miller, M. Moorman, R. Manginell, C. Ashlee, I. Brener, D. Wheeler, et al., Towards an Integrated Microneedle Total Analysis Chip for Protein Detection, Electroanalysis, 28 (2016) 1305–10.

[14] P.P. Samant, M.R. Prausnitz, Mechanisms of sampling interstitial fluid from skin using a microneedle patch, Proceedings of the National Academy of Sciences of the United States of America, 115 (2018) 4583–8.

[15] Y.-C. Kim, J.-H. Park, M.R. Prausnitz, Microneedles for drug and vaccine delivery, Adv Drug Deliv Rev, 64 (2012) 1547–68.

[16] C. Ericsson, M. Nistér, Protein Extraction from Solid Tissue, in: J. Dillner (Ed.) Methods in Biobanking, Humana Press, Totowa, NJ, 2011, pp. 307–12.

[17] N.L. Anderson, Counting the proteins in plasma, Clin Chem, 56 (2010) 1775–6

[18] L. Fuertes, C. Santonja, H. Kutzner, L. Requena, Immunohistochemistry in Dermatopathology: A Review of the Most Commonly Used Antibodies (Part I), Actas Dermo-Sifiliográficas (English Edition), 104 (2013) 99–127.

[19] L.A. Compton, G.F. Murphy, C.G. Lian, Diagnostic Immunohistochemistry in Cutaneous Neoplasia: An Update, Dermatopathology, 2 (2015) 15–42.

[20] S.J. Ohsie, G.P. Sarantopoulos, A.J. Cochran, S.W. Binder, Immunohistochemical characteristics of melanoma, J Cutan Pathol, 35 (2008) 433–44.

[21] M.I. Haq, E. Smith, D.N. John, M. Kalavala, C. Edwards, A. Anstey, et al., Clinical administration of microneedles: skin puncture, pain and sensation, Biomed Microdevices, 11 (2009) 35–47.

[22] J. Gupta, H.S. Gill, S.N. Andrews, M.R. Prausnitz, Kinetics of skin resealing after insertion of microneedles in human subjects, J Control Release, 154 (2011) 148–55.

[23] S.-M. Ahn, R. J Simpson, Body fluid proteomics: Prospects for biomarker discovery, Proteomics Clin Appl (2007) 1004–15.

[24] E.M. Vicente-Perez, E. Larrañeta, M.T.C. McCrudden, A. Kissenpfennig, S. Hegarty, H.O. McCarthy, et al., Repeat application of microneedles does not alter skin appearance or barrier function and causes no measurable disturbance of serum biomarkers of infection, inflammation or immunity in mice in vivo, Eur J Pharm Biopharm, 117 (2017) 400–7.

[25] M.L. Graham, M.J. Prescott, The multifactorial role of the 3Rs in shifting the harm-benefit analysis in animal models of disease, Eur J Pharmacol, 759 (2015) 19–29.

[26] T. Hartung, Thoughts on limitations of animal models, Parkinsonism Relat Disord, 14 Suppl 2 (2008) S81–3.

[27] E. Abd, S.A. Yousef, M.N. Pastore, K. Telaprolu, Y.H. Mohammed, S. Namjoshi, et al., Skin models for the testing of transdermal drugs, Clin Pharmacol: advances and applications, 8 (2016) 163–76.

[28] T. Denayer, T. Stöhr, M. Van Roy, Animal models in translational medicine: Validation and prediction, New Horizons Transl Med, 2 (2014) 5–11.

[29] B. Godin, E. Touitou, Transdermal skin delivery: predictions for humans from in vivo, ex vivo and animal models, Adv Drug Deliv Rev, 59 (2007) 1152–61.

[30] U. Jacobi, M. Kaiser, R. Toll, S. Mangelsdorf, H. Audring, N. Otberg, et al., Porcine ear skin: an in vitro model for human skin, Skin Res Technol, 13 (2007) 19–24.

[31] E.C. Jung, I. Howard, Maibach, Animal Models for Percutaneous Absorption, in: P.V.P. Shah, I.H. Maibach, J. Jenner (Eds.), Topical drug bioavailability, bioequivalence, and penetration, 2 ed., 2014, New York, 2014.

[32] D. Krajnovic, N. Dragicevic, Ethical Conciderations in Research Involving Dermal and Transdermal Drug Delivery, in: N. Dragicevic, H.I. Maibach (Eds.), Percutaneous

Penetration Enhancers Drug Penetration Into/Through the Skin, 1 ed., Springer, Berlin, 2017.

[33] L. Luo, A. Patel, B. Sinko, M. Bell, J. Wibawa, J. Hadgraft, et al., A comparative study of the in vitro permeation of ibuprofen in mammalian skin, the PAMPA model and silicone membrane, Int J Pharm, 505 (2016) 14–9.

[34] T.F. Vandamme, Use of rodents as models of human diseases, J of pharmacy & Bioall Sci, 6 (2014) 2–9.

[35] S. Diridollou, D. Black, J.M. Lagarde, Y. Gall, M. Berson, V. Vabre, et al., Sex- and site-dependent variations in the thickness and mechanical properties of human skin in vivo, Int Journal Cosmet Sci, 22 (2000) 421–35.

[36] J. Sandby-Moller, T. Poulsen, H.C. Wulf, Epidermal thickness at different body sites: relationship to age, gender, pigmentation, blood content, skin type and smoking habits, Acta Derm Venereol, 83 (2003) 410–3.

[37] H. Tagami, M. Ohi, K. Iwatsuki, Y. Kanamaru, M. Yamada, B. Ichijo, Evaluation of the skin surface hydration in vivo by electrical measurement, J Invest Dermatol, 75 (1980) 500–7.

[38] C.H. Daly, G.F. Odland, Age-related changes in the mechanical properties of human skin, J Invest Dermatol, 73 (1979) 84–7.

[39] S. Diridollou, V. Vabre, M. Berson, L. Vaillant, D. Black, J.M. Lagarde, et al., Skin ageing: changes of physical properties of human skin in vivo, Int Journal Cosmet Sci, 23 (2001) 353–62.

[40] S.M. Evans, A.E. Schrlau, A.A. Chalian, P. Zhang, C.J. Koch, Oxygen levels in normal and previously irradiated human skin as assessed by EF5 binding, J Invest Dermatol, 126 (2006) 2596–606.

[41] J.K. Kular, S. Basu, R.I. Sharma, The extracellular matrix: Structure, composition, age-related differences, tools for analysis and applications for tissue engineering, J Tissue Eng, 5 (2014) 2041731414557112.

[42] Q.L. Loh, C. Choong, Three-dimensional scaffolds for tissue engineering applications: role of porosity and pore size, Tissue Eng Part B, Rev, 19 (2013) 485–502.

[43] B. Bedogni, M.B. Powell, Skin hypoxia: a promoting environmental factor in melanomagenesis, Cell Cycle, 5 (2006) 1258–61.

[44] B. Bedogni, M.B. Powell, Hypoxia, melanocytes and melanoma - survival and tumor development in the permissive microenvironment of the skin, Pigment Cell Melanoma Res, 22 (2009) 166–74.

[45] F.J. O'Brien, Biomaterials & scaffolds for tissue engineering, Mater Today, 14 (2011).

[46] B. Dhandayuthapani, Y. Yoshida, ToruMaekawa, D.S. Kumar, Polymeric Scaffolds in Tissue Engineering Application: A Review, Int J Polym Sci, 2011 (2011).

[47] E. Burdett, K. Kasper, A.G. Mikos, J.A. Ludwig, Engineering Tumors: A Tissue Engineering Perspective in Cancer Biology, issue Eng Part B, Rev, 16 (2010) 351–9.

[48] S. Totti, S.I. Vernardis, L. Meira, P.A. Perez-Mancera, E. Costello, W. Greenhalf, et al., Designing a bio-inspired biomimetic in vitro system for the optimization of ex vivo studies of pancreatic cancer, Drug Discov Today, 22 (2017) 690–701.

[49] S. Totti, M.C. Allenby, S.B. Dos Santos, A. Mantalaris, E.G. Velliou, A 3D bioinspired highly porous polymeric scaffolding system for in vitro simulation of pancreatic ductal adenocarcinoma, RSC Adv, 8 (2018) 20928–40.

[50] A.A. Chaudhari, K. Vig, D.R. Baganizi, R. Sahu, S. Dixit, V. Dennis, et al., Future Prospects for Scaffolding Methods and Biomaterials in Skin Tissue Engineering: A Review, Int J Mol Sci, 17 (2016) 1974.

[51] G. Henze, R. Dummer, H.I. Joller-Jemelka, R. Boni, G. Burg, Serum S100--a marker for disease monitoring in metastatic melanoma, Dermatology (Basel, Switzerland), 194 (1997) 208–12.

[52] H.B. Guo, B. Stoffel-Wagner, T. Bierwirth, J. Mezger, D. Klingmuller, Clinical significance of serum S100 in metastatic malignant melanoma, Eur J Cancer, 31a (1995) 1898–902.

[53] R.L. Siegel, K.D. Miller, A. Jemal, Cancer statistics, 2018, CA Cancer J Clin, 68 (2018) 7–30.

[54] American Cancer Society, Cancer Facts and Figures 2019, (2019).

[55] R. Harpio, R. Einarsson, S100 proteins as cancer biomarkers with focus on S100B in malignant melanoma, Clin Biochem, 37 (2004) 512–8.

[56] T.M. Blanco, A. Mantalaris, A. Bismarck, N. Panoskaltsis, The development of a three-dimensional scaffold for ex vivo biomimicry of human acute myeloid leukaemia, Biomaterials, 31 (2010) 2243–51.

[57] E.G. Velliou, S.B.D. Santos, M.M. Papathanasiou, M. Fuentes-Gari, R. Misener, N. Panoskaltsis, et al., Towards unravelling the kinetics of an acute myeloid leukaemia model system under oxidative and starvation stress: a comparison between two- and three-dimensional cultures, Bioprocess Biosyst Eng, 38 (2015) 1589–600.

[58] A. Summerfield, F. Meurens, M.E. Ricklin, The immunology of the porcine skin and its value as a model for human skin, Mol Immunol, 66 (2015) 14–21.

[59] S.H. Bariya, M.C. Gohel, T.A. Mehta, O.P. Sharma, Microneedles: an emerging transdermal drug delivery system, J Pharm Pharmacol, 64 (2012) 11–29.

[60] H. Joodaki, M.B. Panzer, Skin mechanical properties and modeling: A review, Proc Inst of Mech Eng H: Journal of Engineering in Medicine, 232 (2018) 323–43.

[61] A.Z. Alkilani, M.T. McCrudden, R.F. Donnelly, Transdermal Drug Delivery: Innovative Pharmaceutical Developments Based on Disruption of the Barrier Properties of the stratum corneum, Pharmaceutics, 7 (2015) 438–70.

[62] A. Kalra, A.-J. AM, Mechanical Nehaviour of Skin: A Review, J Material Sci Eng, 5 (2016).

[63] S.F. Altschul, T.L. Madden, A.A. Schaffer, J. Zhang, Z. Zhang, W. Miller, et al., Gapped BLAST and PSI-BLAST: a new generation of protein database search programs, Nucleic Acids Res, 25 (1997) 3389–402.

[64] B. Bandarchi, L. Ma, R. Navab, A. Seth, G. Rasty, From melanocyte to metastatic malignant melanoma, Dermatol Res Pract, 2010 (2010).

[65] S. Avram, D.E. Coricovac, I.Z. Pavel, I. Pinzaru, R. Ghiulai, F. Baderca, et al., Standardization of A375 human melanoma models on chicken embryo chorioallantoic membrane and Balb/c nude mice, Oncol Rep, 38 (2017) 89–99.

[66] A.M. Barsotti, M. Ryskin, W. Zhong, W.G. Zhang, A. Giannakou, C. Loreth, et al., Epigenetic reprogramming by tumor-derived EZH2 gain-of-function mutations promotes aggressive 3D cell morphologies and enhances melanoma tumor growth, Oncotarget, 6 (2015) 2928–38.

[67] L. Gibot, T. Galbraith, J. Huot, F.A. Auger, Development of a tridimensional microvascularized human skin substitute to study melanoma biology, Clin Exp Metastasis, 30 (2013) 83–90.

[68] K. Klimkiewicz, K. Weglarczyk, G. Collet, M. Paprocka, A. Guichard, M. Sarna, et al., A 3D model of tumour angiogenic microenvironment to monitor hypoxia effects on cell interactions and cancer stem cell selection, Cancer Lett, 396 (2017) 10–20.

[69] B. Marrero, J.L. Messina, R. Heller, Generation of a tumor spheroid in a microgravity environment as a 3D model of melanoma, In vitro Cell Dev Biol Anim, 45 (2009) 523–34.

[70] O.F. Kandarakov, M.V. Kalashnikova, A.A. Vartanian, A.V. Belyavsky, Homogeneous and heterogeneous in vitro 3D models of melanoma, Mol Biol, 49 (2015) 895–8.

[71] D.S. Hill, N.D.P. Robinson, M.P. Caley, M. Chen, E.A. O'Toole, J.L. Armstrong, et al., A novel fully-humanised 3D skin equivalent to model early melanoma invasion, Mol Cancer Ther, 14 (2015) 2665–73.

[72] E. Knight, B. Murray, R. Carnachan, S. Przyborski, Alvetex(R): polystyrene scaffold technology for routine three dimensional cell culture, Methods in molecular biology (Clifton, NJ), 695 (2011) 323–40.

[73] C.C. Compton, D.R. Byrd, J. Garcia-Aguilar, S.H. Kurtzman, A. Olawaiye, M.K. Washington, Melanoma of the Skin, in: C.C. Compton, D.R. Byrd, J. Garcia-Aguilar, S.H. Kurtzman, A. Olawaiye, M.K. Washington (Eds.), AJCC Cancer Staging Atlas: A Companion to the Seventh Editions of the AJCC Cancer Staging Manual and Handbook, Springer New York, New York, NY, 2012, pp. 385–416.

[74] A.R. Bresnick, D.J. Weber, D.B. Zimmer, S100 proteins in cancer, Nat Rev Cancer, 15 (2015) 96.

[75] S. Mocellin, G. Zavagno, D. Nitti, The prognostic value of serum S100B in patients with cutaneous melanoma: A meta-analysis, Int J Cancer, 123 (2008) 2370–6.

[76] R. Donato, S-100 proteins, Cell calcium, 7 (1986) 123–45.

[77] R. Donato, Perspectives in S-100 protein biology. Review article, Cell calcium, 12 (1991) 713–26.

[78] D.B. Zimmer, E.H. Cornwall, A. Landar, W. Song, The S100 protein family: history, function, and expression, Brain Res Bull, 37 (1995) 417–29.

[79] A. Díaz-Lagares, E. Alegre, A. Arroyo, M. González-Cao, M.E. Zudaire, S. Viteri, et al., Evaluation of multiple serum markers in advanced melanoma, Tumor Biol, 32 (2011) 1155.

[80] A. Bolander, M. Agnarsdottir, G. Wagenius, S. Stromberg, F. Ponten, S. Ekman, et al., Serological and immunohistochemical analysis of S100 and new derivatives as markers for prognosis in patients with malignant melanoma, Melanoma Res, 18 (2008) 412–9.

[81] K. Müller, A. Elverland, B. Romner, K. Waterloo, B. Langbakk, J. Undén, et al., Analysis of protein S-100B in serum: a methodological study, Clin Chem Lab Med (CCLM) 2011, p. 1111.

[82] H. Haslene-Hox, A. Madani, K.C.G. Berg, K. Woie, H.B. Salvesen, H. Wiig, et al., Quantification of the concentration gradient of biomarkers between ovarian carcinoma interstitial fluid and blood, BBA Clinical, 2 (2014) 18–23.

[83] G. Cevc, G. Blume, Lipid vesicles penetrate into intact skin owing to the transdermal osmotic gradients and hydration force, Biochim Biophys Acta, 1104 (1992) 226–32.

[84] L. Safinia, A. Mantalaris, A. Bismarck, Nondestructive technique for the characterization of the pore size distribution of soft porous constructs for tissue engineering, Langmuir, 22 (2006) 3235–42.